

Structural Evolution of Colloidal Crystal Films in the Process of Melting Revealed by Bragg Peak Analysis

Elena A. Sulyanova,^{†,‡} Anatoly Shabalin,[†] Alexey V. Zozulya,^{*,†} Janne-Mieke Meijer,[§] Dmitry Dzhigaev,^{†,||} Oleg Gorobtsov,^{†,⊥} Ruslan P. Kurta,[#] Sergey Lazarev,^{†,∇} Ulf Lorenz,[○] Andrej Singer,[◆] Oleksandr Yefanov,^{||} Ivan Zaluzhnyy,^{†,||} Ilya Besedin,^{†,||} Michael Sprung,[†] Andrei V. Petukhov,[§] and Ivan A. Vartanyants^{*,†,||}

[†]Deutsches Elektronen-Synchrotron DESY, Notkestraße 85, D-22607 Hamburg, Germany

[‡]Shubnikov Institute of Crystallography RAS, Leninskii pr. 59, 119333 Moscow, Russia

[§]Van 't Hoff laboratory for Physical and Colloid Chemistry, Debye Institute for Nanomaterials Science, Utrecht University, Padualaan 8, 3508 TB Utrecht, The Netherlands

^{||}National Research Nuclear University MEPhI (Moscow Engineering Physics Institute), Kashirskoye ch. 31, 115409 Moscow, Russia

[⊥]NRC Kurchatov Institute, Akademika Kurchatova pl. 1, 123182 Moscow, Russia

[#]European XFEL GmbH, Albert-Einstein-Ring 19, D-22761 Hamburg, Germany

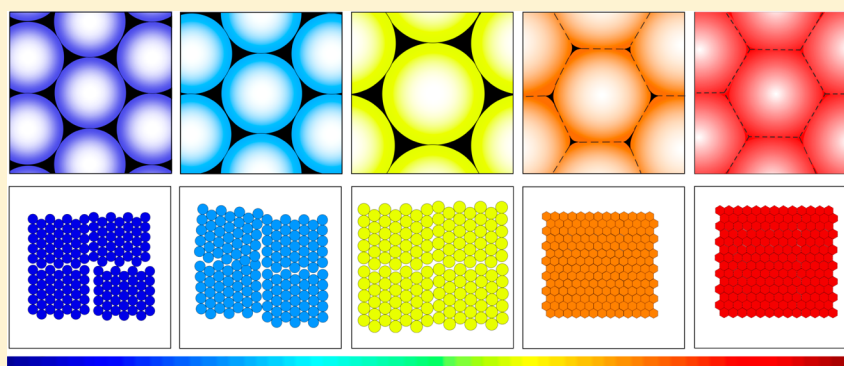
[∇]National Research Tomsk Polytechnic University (TPU), Lenina pr. 2a, 634028 Tomsk, Russia

[○]Department of Chemistry, University of Potsdam, D-14476 Potsdam, Germany

[◆]University of California San Diego, 9500 Gilman Dr., La Jolla, California 92093, United States

^{||}Center for Free-Electron Laser Science, DESY, Notkestraße 85, D-22607 Hamburg, Germany

S Supporting Information



ABSTRACT: In situ X-ray diffraction studies of structural evolution of colloidal crystal films formed by polystyrene spherical particles upon incremental heating are reported. The Bragg peak parameters, such as peak position, integrated intensity, and radial and azimuthal widths were analyzed as a function of temperature. A quantitative study of colloidal crystal lattice distortions and mosaic spread as a function of temperature was carried out using Williamson–Hall plots based on mosaic block model. The temperature dependence of the diameter of polystyrene particles was obtained from the analysis of Bragg peaks, and the form factor contribution extracted from the diffraction patterns. Four stages of structural evolution in a colloidal crystal upon heating were identified. Based on this analysis, a model of the heating and melting process in the colloidal crystal film is suggested.

1. INTRODUCTION

Due to the existence of photonic band gaps, periodic photonic nanostructures are considered to be the optical analogue of electronic semiconductors and can significantly affect light emission and propagation.¹ These materials are expected to be an important part of future optical communication lines and are of special interest in sensor technology and data storage. Colloidal crystals formed by self-assembly of submicrometer colloidal spherical particles^{2,3} are especially attractive materials

for these applications due to the possibility of covering large areas, designed shape, and low production cost. Occasional appearance of defects in a photonic crystal leads to significant degradation of its optical characteristics.⁴ Investigation of a real structure of these materials and its temperature dependence is

Received: December 2, 2014

Revised: January 16, 2015

Published: January 16, 2015

therefore important for the future development of photonic devices.

In the process of self-assembled growth of a colloidal crystal on a substrate, the colloidal spherical particles form a close-packed structure. There are two well-known periodic close-packed arrangements of spheres: face-centered cubic (fcc) and hexagonal close-packed (hcp) structures.⁵ The free energy difference between fcc and hcp structures is very small.⁶ During the self-organized growth of colloidal crystal film the structure of a film often represents a mixture of these two lattices referred to as random hexagonal close-packed structure (rhcp).^{7,8} This means that defects are intrinsically present in colloidal crystals and can be considered as one of the challenges in the manufacturing of high-quality photonic devices based on self-assembled colloidal crystals.

The structure of colloidal systems can be examined in different ways. Among widely used techniques are optical microscopy^{9,10} and, especially, confocal laser scanning microscopy.¹¹ These methods, however, are severely limited in terms of their resolution. Scanning electron microscopy (SEM) can provide high spatial resolution; however, due to low penetration depth of electrons, SEM can only access the surface structure of a colloidal crystal and typically involves elaborate sample preparation.¹² In this respect small-angle X-ray scattering (SAXS)¹³ and small-angle neutron scattering (SANS)¹⁴ represent complementary methods offering the advantage of high penetration depth for nondestructive studies of colloidal systems. However, the unit cell in colloidal crystals is about a few hundreds of nanometers in size, which is more than three orders of magnitude larger than the wavelength of X-rays or neutrons, thus making the experimental studies quite challenging. In comparison to SANS, the synchrotron based SAXS exploits highly intense and collimated X-ray beams, which provides microradian resolution.¹⁵ The latter is essential for the characterization of the long-range positional order in colloidal crystals.^{8,16,17} Latest studies using coherent X-ray diffraction have shown possibilities for *ab initio* reconstruction of two-dimensional (2D) and three-dimensional (3D) arrangements of colloidal spheres in a crystal.^{18–20}

An important aspect of possible applications of colloidal systems in photonics and nanolithography is their behavior under heating and annealing treatment.^{21–28} Structural studies of spin-coated polystyrene (PS) colloidal thin films during annealing using a combination of grazing incidence small-angle X-ray scattering and optical ellipsometry have been reported by Herzog et al.²⁷ It was observed that colloidal particles flatten during annealing, and it was suggested²⁵ that a coalescence process takes place. Similar observations were made in the work of Chen et al.²⁶ where the structural evolution of latex films was studied as a function of annealing time using SAXS. Two main effects due to dry sintering were identified: particle deformation and aggregation of particles due to interdiffusion of polymer chains.

Presently, it is not well studied what happens with a 3D assembly of colloidal particles in a crystal upon heating. We can generally assume that the glass transition temperature of the polymer should directly influence the melting temperature of the colloidal crystal. An effect of heat treatment on PS colloidal crystal films grown by vertical deposition was first investigated in our previous work.²⁹ By monitoring the X-ray diffraction patterns in transmission geometry and following the diffuse scattering distribution upon heating, it was found that, before

the complete loss of crystal order, the colloidal particles undergo a transformation from spherical to a faceted shape.

In the present work, we aim at a quantitative investigation of lattice distortions and particle shape changes in colloidal crystals upon heating treatment. For this purpose, we perform a detailed analysis of Bragg peaks in diffraction patterns of PS colloidal crystals measured *in situ* during incremental heating.

2. EXPERIMENTAL SECTION

PS colloidal crystal films were prepared using the vertical deposition method.^{17,30} PS spheres were obtained by polymerization of the aqueous solution of styrene using potassium persulfate as the initiator. The obtained atactic polymer with no control of the side group orientation possesses the typical glass transition temperature T_G of about 373 K.³¹ Polydispersity of colloidal particles as measured by dynamic light scattering (DLS) was 2.1%. Thin glass substrates were inserted into colloidal suspensions contained particles at 1% volume fraction in water and subsequently dried at 323 K for at least 24 h. The grown colloidal crystal films consisted of 40–50 monolayers of PS spherical particles, depending on the position on a film along the growth direction. Typically, the colloidal crystal films exhibit a cracked texture consisting of single-crystal regions with an average size of several tens of micrometers (as shown in the inset of Figure 1).

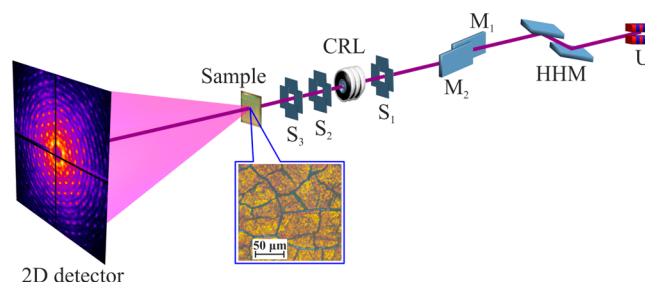


Figure 1. Schematic view of the experimental setup: U, undulator source; HHM, high heat load monochromator; M_1 , M_2 , pair of flat X-ray mirrors; S_1 , S_2 , S_3 , slit systems; CRL, compound refractive lenses. Inset at the sample position: an optical micrograph of the colloidal crystal.

X-ray diffraction experiments were performed at the Coherence Beamline P10 of the PETRA III synchrotron facility at DESY, Hamburg. A sketch of the experimental setup is shown in Figure 1. The synchrotron beam from the undulator source (U) was monochromatized by a high heat load monochromator (HHM) exploiting Si(111) reflection. A pair of flat Si-coated mirrors (M_1 , M_2) was used to reject higher harmonics from the undulator spectrum. The slit system (S_1) was used to define the beam size at the entrance of focusing optics. The focusing optics based on compound refractive lenses (CRLs) can be optionally inserted in the beam path at 1.57 m distance upstream the sample position.³² Two collimating slits (S_2 , S_3) were located at 0.8 and 0.3 m upstream a sample and were used to define the size of unfocused beam. The sample was positioned inside a vacuum chamber at 87.7 m distance from the source. Diffraction patterns were recorded by using the 2D detector MAXIPIX with total area of 516×516 pixels and a pixel size of $55 \times 55 \mu\text{m}^2$. The detector was positioned at 5.1 m distance downstream the sample. To eliminate parasitic background due to air scattering, an evacuated flight tube was used between sample and detector. In order to protect the detector from the primary beam, the beamstop made of a tungsten cylinder of 3 mm diameter was positioned inside the flight tube.

The glass substrates of colloidal samples were cut to $3 \times 6 \text{ mm}^2$ pieces and mechanically attached to a copper holder plate. The copper plate was fixed to a copper block designed as an insert flange of the sample chamber. The heating of the copper block was supplied via two heating elements connected in parallel and built in the copper block. To provide controlled heat exchange, the copper block with heating

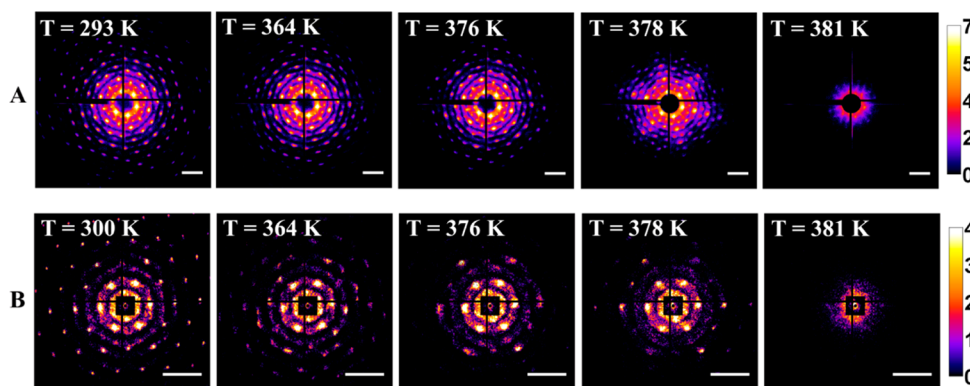


Figure 2. X-ray diffraction patterns measured in situ during incremental heating of the PS colloidal crystals in experiments A (top row) and B (bottom row) (see text for details). Intensity values are presented in logarithmic color scale. Scale bar shown for each pattern is $50 \mu\text{m}^{-1}$.

elements was separated by a Peltier element from the outer copper part. The latter was connected to a water cooling cycle and acted as a heat sink. The temperature of the sample holder was monitored using two PT100 temperature sensors integrated in the copper block. Temperature and heating power were adjusted using a LakeShore 340 temperature controller. The temperature of the samples was increased incrementally starting from room temperature ($T_R = 293 \text{ K}$). Prior to the data collection, a waiting time of 5 min was applied at each temperature to reach thermal equilibrium.

We performed two X-ray diffraction experiments (denoted below as experiment A and experiment B) on PS colloidal crystal films grown in similar conditions, but consisting of spherical particles with different size. For both experiments, the size of PS colloidal particles at room temperature was determined by transmission electron microscopy (TEM) and by the Bragg peak and form factor analysis performed in this work (see Table 1).

Table 1. Diameter of PS Spherical Particles D and Average Lattice Parameter $\langle a_{[110]} \rangle$ Determined by Different Methods at Room Temperature

experiment	particle diameter D , nm		average lattice parameter $\langle a_{[110]} \rangle$, nm
	TEM	form factor analysis (this work)	Bragg peak analysis (this work)
A	415 ± 8	416 ± 0.2	417 ± 1
B	386 ± 8		392 ± 2

Experiment A was performed at a photon energy of 15 keV using an unfocused beam of $50 \times 50 \mu\text{m}^2$ in size, which was chosen to approximately match the single-crystal domain area in a colloidal crystal. At each temperature value, data were collected from the same position on a sample by acquiring a series of 300 frames with exposure time of 0.03 s per frame. The resulting diffraction patterns were obtained by summing up all frames in a series.

The conditions of experiment B were chosen in order to collect ptychographic coherent diffraction patterns from the PS colloidal crystal. Ptychography^{33,34} is a recently developed coherent diffraction imaging technique which enables the study of extended objects with coherent X-rays and involves the scanning of the object in an X-ray beam across the desired field of view. The analysis of ptychographic data collected in experiment B will be reported in a separate publication. In this experiment, a photon energy of 8 keV was selected and the beam was focused at the sample position to a spot size of $2.8(\text{v}) \times 3.5(\text{h}) \mu\text{m}^2$ (vertical \times horizontal) using the CRL focusing optics. To obtain a high degree of transverse coherence in the focused beam, the entrance slits (S_1) in front of the CRL optics were set to a size of $100(\text{v}) \times 75(\text{h}) \mu\text{m}^2$. In order to collect data over a large sample area, the diffraction patterns were measured by raster scanning of a sample on a rectangular grid with $1 \mu\text{m}$ step size over 11×11

points and acquiring five frames of 0.5 s exposure at each scanned point. Under these experimental conditions, the resolution values in reciprocal space as defined by the incoming beam divergence and photon energy were 0.43 and $2.49 \mu\text{m}^{-1}$ for experiments A and B, respectively.

3. RESULTS

The diffraction patterns measured in experiments A and B under incremental heating of PS colloidal crystals are shown in Figure 2. Due to the relatively large unit cell of the colloidal crystals, a number of Bragg peaks can be observed in a single diffraction pattern measured in transmission geometry. In experiment A, Bragg peaks up to the 11th diffraction order were observed at room temperature. For lower photon energy used in experiment B, we observed seven diffraction orders at room temperature. Due to high spatial coherence of the incoming focused beam used in experiment B, the observed diffraction peaks were broadened and had a complicated internal structure known as X-ray speckles³⁵ (see Figure 2, bottom row). Speckles are produced when the illuminating beam is highly coherent and different regions of the sample introduce different phase shifts. The average speckle size is inversely proportional to the coherently illuminated area of a sample, which is defined by the beam size. Speckle features were not present in the diffraction patterns of experiment A where partially coherent illumination was used.

Inspection of the diffraction patterns presented in Figure 2 shows that at temperatures below glass transition temperature T_G there are no strong changes in the structure of diffraction peaks. Only a slight decrease of intensity of higher order Bragg peaks can be observed at elevated temperatures. However, at $T > T_G$, the diffraction patterns evolve very rapidly with temperature. Higher order diffraction peaks gradually decrease in their intensity which indicates the decay of long-range order in the colloidal crystal upon heating. Additionally, we observed a 6-fold modulation of both the intensity of Bragg peaks and the diffuse scattering background in diffraction patterns for experiment A (see Figure 2, top row, $T = 378 \text{ K}$). This indicates that spherical particles in a colloidal crystal transform to a faceted shape upon dry sintering.

In addition to Bragg peaks, distinct intensity modulations appearing as concentric rings can be observed in the experimental diffraction patterns. These modulations originate from the form factor of a spherical colloidal particle. We extracted the form factor contributions averaged over azimuthal angle for each of the experimental diffraction patterns (see Appendix A in the Supporting Information for details of an

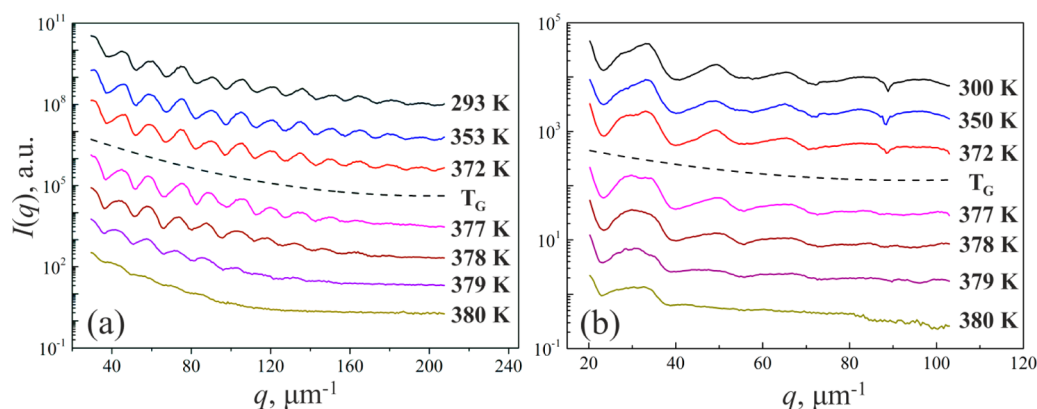


Figure 3. Temperature evolution of the form factor curves $I(q)$ of PS spherical particles measured from colloidal crystal samples in experiment A (a) and experiment B (b). The glass transition temperature of PS $T_G = 373$ K is indicated by the dashed curve.

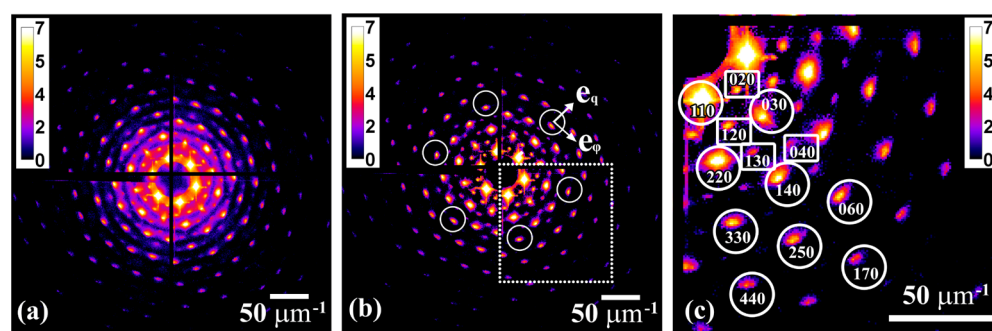


Figure 4. (a) X-ray diffraction pattern measured in experiment A at room temperature. (b) Same pattern after subtracting the form factor contribution. (c) Enlarged area of the diffraction pattern highlighted by the dashed square in (b). The analyzed fcc and rhcp peaks are marked by circles and rectangles, respectively. Intensity levels are presented in logarithmic color scale.

analysis of form factor curves). The form factor curves of PS spherical particles measured from colloidal crystal samples at different temperatures during heating are presented in Figure 3 for both experiments. On the one hand, one can observe large number of intensity oscillations in these curves at room temperature. This means that the colloidal particles under study can be well described as hard spheres with a narrow size distribution. On the other hand, the contrast of intensity oscillations of the form factor curves at high q -values decreases with temperature. This effect can be induced by the particle deformation toward nonspherical shape as well as the broadening of a size distribution of particles.

In order to improve the accuracy of an analysis of Bragg peaks, the scattering signal corresponding to the form factor contribution was subtracted from measured diffraction patterns (see Figure 4). The resulting diffraction patterns contain the diffraction peaks typical for reflections present in colloidal crystals fabricated by vertical deposition technique. Such crystals often consist of stacked hexagonal close-packed layers which are parallel to the substrate and contain some degree of stacking disorder.¹⁷

The following nomenclature of Bragg peaks indexing was adopted. We consider a hexagonal lattice with the crystal lattice vectors \mathbf{a} and \mathbf{b} lying in the colloidal crystal film and vector \mathbf{c} normal to the film. For the transmission geometry shown in Figure 1, an incident beam is perpendicular to the colloidal crystal film, and the Miller index l is always zero. Thus, only indexes h and k can be used for Bragg peak indexing. We will distinguish the two types of $hk0$ reflections: when $(h-k)$ is divisible by three (as indicated in Figure 4c by circles) and

when $(h-k)$ is not divisible by three (as indicated in Figure 4c by squares).²⁰ The reflections of the first type have higher intensity and are stacking-independent, which will be referred as fcc reflections. The reflections of the second type are induced by stacking disorder. These are weaker and will be referred as rhcp reflections. For experiment A, the total number of nine orders of fcc Bragg peaks were considered for the analysis (see Figure 4c), and for experiment B four fcc orders were analyzed. For both experiments, four orders of rhcp Bragg peaks were evaluated.

4. DISCUSSION

To investigate the structural evolution of PS colloidal crystals during heating, we performed a detailed analysis of the measured diffraction patterns shown in Figure 2. The following four parameters of Bragg peaks as a function of temperature were analyzed: Bragg peak position q_B , integrated intensity, and full widths at half-maximum (FWHMs) in radial (w_q) and azimuthal (w_φ) directions in reciprocal space. The details of the data processing and Bragg peak evaluation procedures are given in Appendix B in the Supporting Information. The results of Bragg peak analysis for experiments A and B are shown in Figures 5 and 6, respectively. The determined widths of Bragg peaks for experiment B were corrected for the instrumental broadening (see Appendix B in the Supporting Information for details), while for experiment A such a correction was negligible.

According to our results, we can identify four stages of structural evolution of PS colloidal crystals upon heating which are indicated in Figures 5 and 6 as regions I, II, III, and IV. In

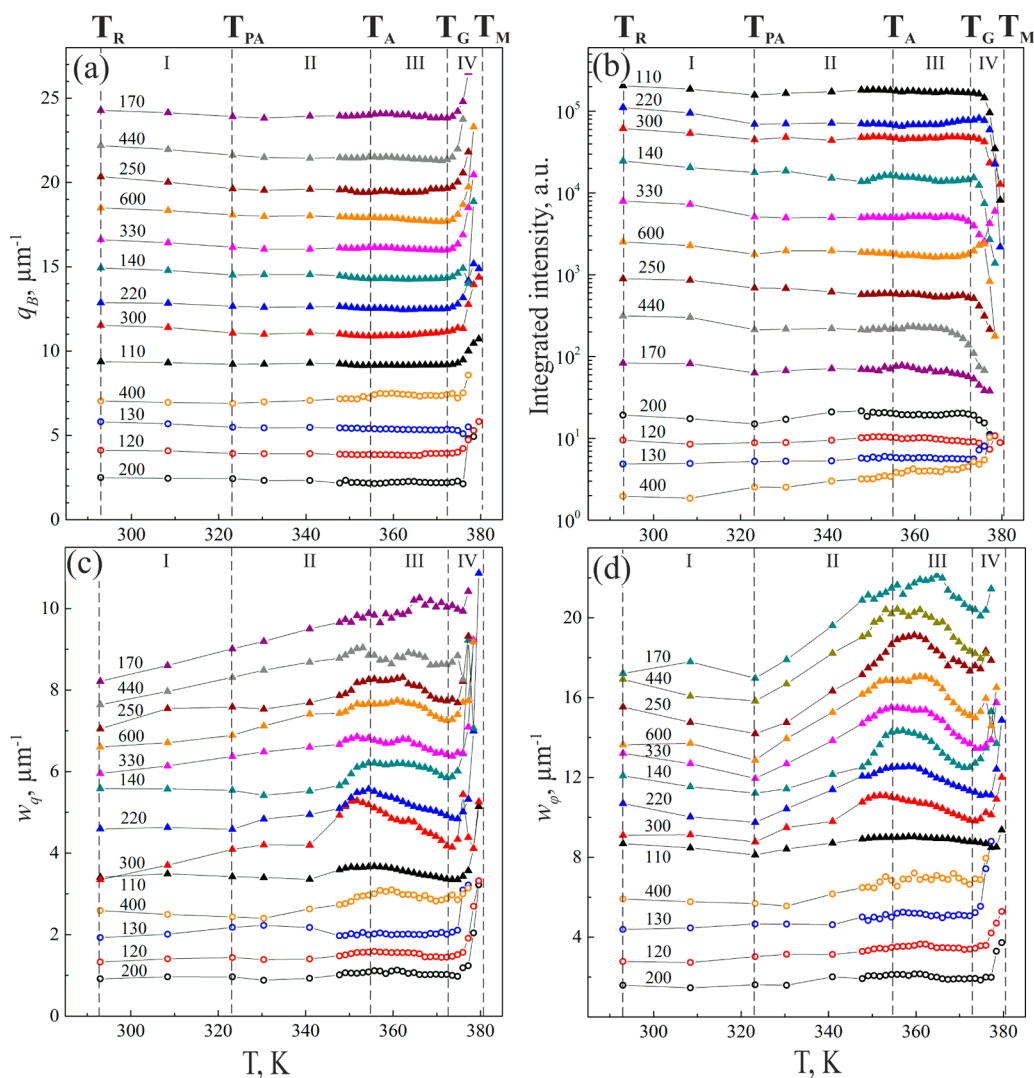


Figure 5. Experiment A. Temperature evolution of Bragg peak parameters: peak positions q_B (a), integrated intensities (b), and FWHMs in radial w_q (c) and azimuthal w_ϕ (d) directions. For visibility, all curves were shifted vertically. Reflections of fcc and rhcp types are displayed by triangles and circles, respectively. The curves in (a), (c), and (d) are arranged in the ascending order of the momentum transfer value q ; the curves in (b) are in the descending order of the q value.

the first stage of heating from room temperature to preannealing temperature, $T_{PA} = 323$ K, no significant variations of peak parameters can be observed. The peak positions q_B slightly decrease due to thermal expansion of the crystal lattice. Interestingly, in this region, the width of higher order peaks in the radial direction (w_q) increases with the increase of the temperature, while the width in the azimuthal direction (w_ϕ) decreases. This indicates a slight increase of the lattice positional disorder along with an annealing effect when crystalline domains become more angular ordered in the plane of a film.

The second stage corresponds to the temperature range between T_{PA} and annealing temperature $T_A = 355$ K. Within this stage, the Bragg peak positions q_B for both experiments continue to decrease. For experiment A, this decrease is about $0.9 \pm 0.5 \mu\text{m}^{-1}$, which means that the crystal lattice expands by about 1% within the second stage of heating treatment. The strongest changes are observed in the temperature evolution of FWHMs of Bragg peaks in the radial and azimuthal directions $w_{q,\phi}$ (see Figures 5c,d and 6c,d). Both parameters strongly increase to a maximum at annealing temperature $T_A = 355$ K.

At this temperature, the maximum values of w_q and w_ϕ exceed the room temperature values by 15–50%. This increase of peak widths indicates a strong enhancement of the lattice disorder and mosaic spread in the colloidal crystal film at these temperatures. The second temperature range can be referred to as preannealing stage.³⁶

The third stage corresponds to the temperature interval from T_A to T_G . In this temperature interval, the peak widths $w_{q,\phi}$ drop down from their maximum values, reaching a local minimum at about T_G (see Figures 5c,d and 6c,d). The decrease of peak widths at $T_A < T < T_G$ is apparently caused by the relaxation of a PS crystal film and the reduction of the structural disorder due to annealing.

In the last stage of heating from T_G to the melting temperature $T_M = 381$ K, the PS colloidal crystal film undergoes a fast melting transition. The melting process occurs in a narrow temperature range and ends finally when the Bragg peaks completely disappear at a temperature of T_M . Within this stage, the peak positions q_B increase rapidly and integrated intensities sharply decrease (see Figures 5a,b and 6a,b). We attribute this behavior to a coalescence of PS colloidal particles

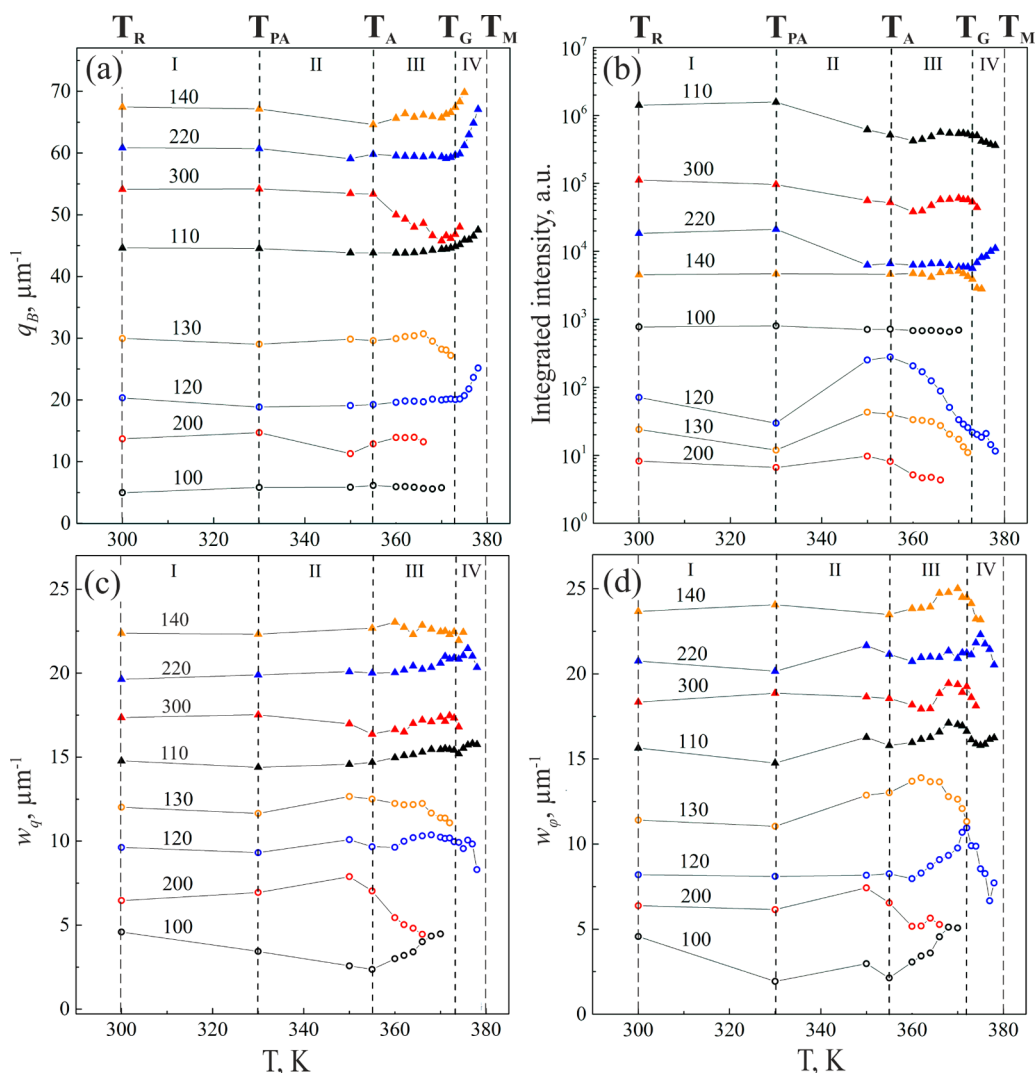


Figure 6. Experiment B. Temperature evolution of Bragg peak parameters: peak positions q_B (a), integrated intensities (b), and FWHMs in radial w_q (c) and azimuthal w_ϕ (d) directions. For visibility, all curves were shifted vertically. Reflections of fcc and rhcp types are displayed by triangles and circles, respectively. The curves in (a), (c), and (d) are arranged in the ascending order of the momentum transfer value q ; the curves in (b) are in the descending order of the q value.

taking place with the increase of temperature. This is further confirmed by the reduction of interparticle distances as it will be seen from the discussion below.

To perform a quantitative analysis of disorder in colloidal crystal films induced by the thermal treatment we applied the Williamson–Hall (WH) method³⁷ based on a mosaic block model to our Bragg peak evaluation. This method assumes that the size $L_{q,\phi}$ of the coherently scattering domain (CSD) and the lattice distortions $g_{q,\phi}$ provide independent contributions to the total width $w_{q,\phi}$ of a Bragg peak. For a normal distribution of these parameters, the following relation holds for the total width of a diffraction peak³⁸

$$w_{q,\phi}^2(q) = \left(\frac{2\pi}{L_{q,\phi}} \right)^2 + (g_{q,\phi} q)^2 \quad (1)$$

The WH method was applied to four orders of $hh0$ reflections measured in experiment A (see Figure 7a,b). The FWHM values used in this analysis were obtained as a result of averaging over six equivalent crystallographic directions.

The average values of lattice distortions (g_q), domain misorientations (g_ϕ), and size of CSDs ($L_{q,\phi}$) as a function of temperature are presented in Figure 7c,d. As can be seen in Figure 7c, the temperature evolution of the lattice distortions (g_q) and domain misorientations (g_ϕ) exhibits the four well distinguished temperature intervals discussed earlier. In the first stage, we observe a slight increase of lattice distortions by about 30% and simultaneous decrease of domain misorientations by about the same amount. In the preannealing stage, both parameters g_q and g_ϕ exhibit especially strong changes: they steadily increase and reach their maxima at the annealing temperature $T_A = 355$ K. The maximal values of parameters g_q and g_ϕ exceed the corresponding room temperature values by almost 100%.

The third stage exhibits decrease of parameters g_q and g_ϕ due to a partial annealing process up to the glass transition temperature $T_G = 373$ K. At the same time the size of CSDs ($L_{q,\phi}$) stays almost constant within the whole temperature range. Both domain sizes were determined to be in the range of 3–5 μm .

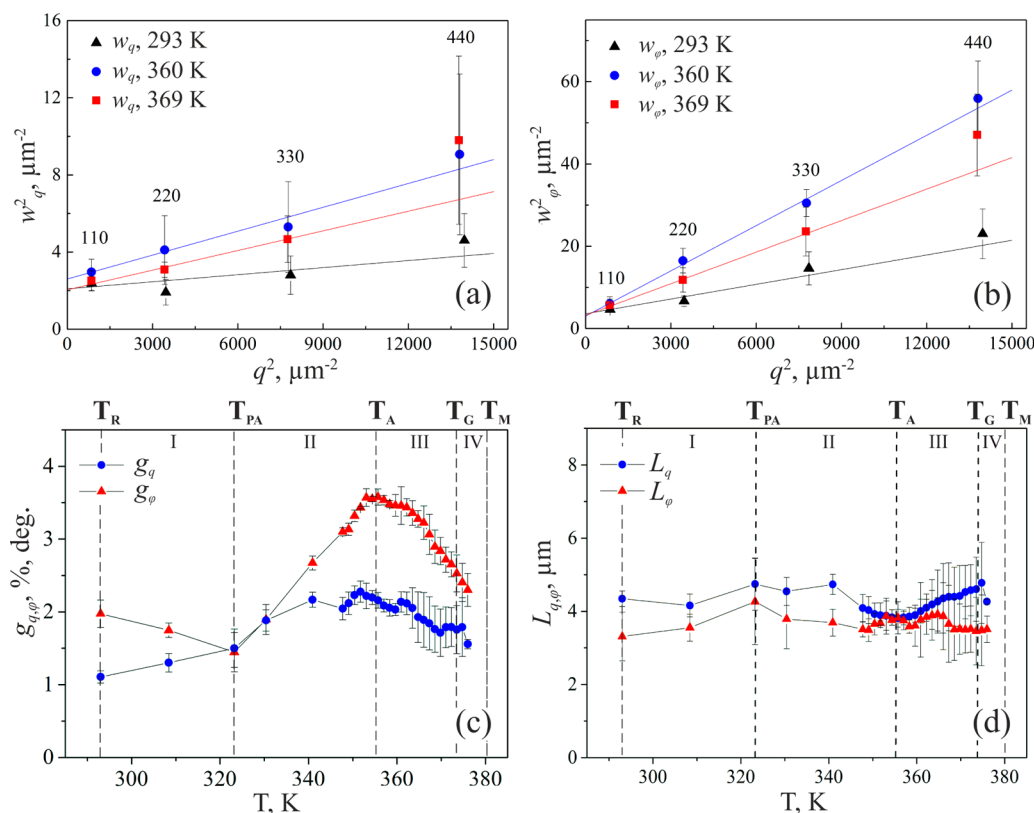


Figure 7. (a, b) Williamson–Hall plots obtained using FWHMs of four orders of fcc reflections in radial (a) and azimuthal (b) directions at different temperatures. Solid lines in (a) and (b) represent linear fits to the experimental data. (c) Temperature dependence of the lattice parameter g_q (in percent) and domain misorientation parameter g_ϕ (in degrees). (d) Temperature dependence of the averaged size of CSD $L_{q,\phi}$.

Domain sizes evaluated in experiment A prevented us from applying the WH method to experiment B because the illuminated spot on a sample of a few micrometers was about the size of a CSD. Under these conditions, the measured data contain no statistical averaging and WH method could not provide adequate information.

To determine the temperature evolution of the size of PS spherical particles, we performed an analysis of the form factor curves obtained from experiment A and shown in Figure 3a. With an assumption of hard sphere model, we obtained a linear growth of the particle diameter from the room temperature to glass transition temperature T_G (see Figure 8). The value of thermal expansion coefficient of $(6.96 \pm 0.35) \times 10^{-5} \text{ K}^{-1}$ was determined from the results of linear fitting. The obtained value is in excellent agreement with the thermal expansion value of $7 \times 10^{-5} \text{ K}^{-1}$ reported in literature.³⁹ However, at higher temperatures, $T > T_G$, it was not possible to obtain reliable results in the frame of the hard sphere model. We attribute this to the softening of boundaries and shape transformation of initially spherical particles, which was not taken into account in our fitting procedure. Unfortunately, it was not possible to perform similar analysis of the form factor data for experiment B (Figure 3b) that we attribute to instrumental broadening of Bragg peaks due to beam focusing and higher polydispersity of colloidal particles in this particular sample.

We determined the temperature evolution of an average lattice parameter $\langle a_{[110]} \rangle$ for the [110] crystallographic direction in our colloidal sample shown in Figure 8 by analyzing equivalent $hh0$ reflections (see Appendix B in the Supporting Information for details). As it follows from our analysis, the average lattice parameter value $\langle a_{hh0} \rangle = 417 \pm 1$

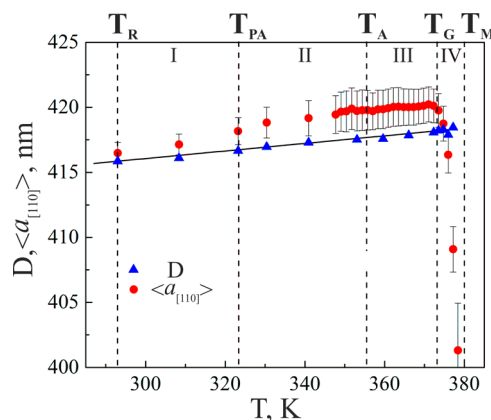


Figure 8. Temperature evolution of the PS particle diameter D (shown by blue triangles) and average lattice parameter $\langle a_{[110]} \rangle$ in [110] crystallographic direction (shown by red circles) for experiment A. Thermal expansion function fitted to $D(T)$ is shown by a solid line. The coefficient of linear thermal expansion of PS was determined to be $(6.96 \pm 0.35) \times 10^{-5} \text{ K}^{-1}$. Error bars for the particle diameter D are within the symbol size.

nm at room temperature is slightly larger than the particle diameter D determined from the form factor data (see Table 1). In the temperature range $T_R < T < T_A$, the lattice parameter first increases slightly faster and after T_A changes linearly according to the temperature expansion law of PS spheres (Figure 8). However, after reaching the glass transition temperature T_G , the lattice parameter drops down rapidly, indicating a fast shrinkage of the colloidal crystal lattice and coalescence of colloidal particles.

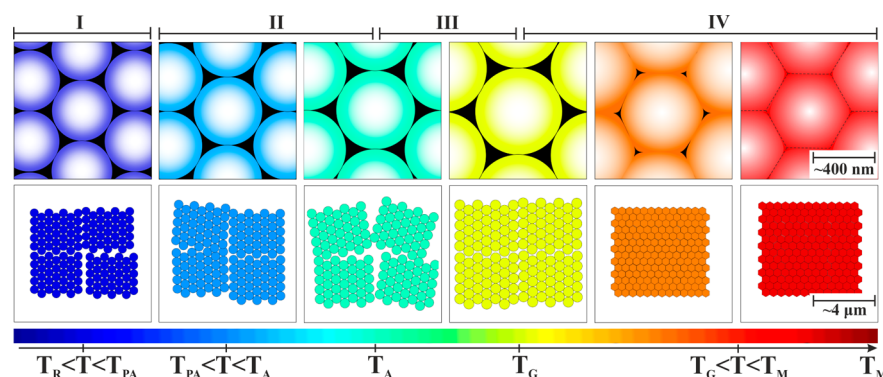


Figure 9. Schematic diagram of the structural evolution in a colloidal crystal film under incremental heating at nanoscopic (top row) and mesoscopic (bottom row) length scales.

Our analysis of the Bragg peaks and form factor curves suggests the following model of the colloidal crystal evolution during incremental heating (see Figure 9). Two length scales, nanoscopic and mesoscopic, need to be considered. The nanoscopic length scale is about the size of a colloidal particle that is in the range of few hundred nanometers in our case (Figure 9, top row). The mesoscopic length scale is related to the size of a coherently scattering domain that is about a few micrometers for colloidal crystals under study (Figure 9, bottom row).

On the nanoscopic length scale, we observed linear growth of the average lattice parameter in the wide temperature range $T_R < T < T_G$ that is directly induced by the thermal expansion of closed packed colloidal spheres (see Figure 8). At temperatures higher than T_G , the PS particles soften and change their shape by flattening in the directions where they touch each other (see Figure 9), that leads to the observation of six-fold symmetry in the diffraction pattern shown in Figure 2 (top row at $T = 378$ K). At the same time, this process is statistical in nature and each particle is deformed differently, that leads to the decrease of the long-range order in the crystalline film and is observed as a decrease of intensity of higher order Bragg peaks with the raise of the temperature (see Figure 2, $T > 376$ K). At higher temperatures, $T > T_G$, the lattice parameter rapidly decreases that indicates fast shrinkage of the lattice until the crystalline structure completely disappears at the melting temperature $T_M = 381$ K.

On the mesoscopic length scale of a few micrometers, we did not observe any particular changes in the temperature interval $T_R < T < T_{PA}$, while for higher temperatures $T_{PA} < T < T_G$ the structure of the colloidal film undergoes significant changes (see Figure 7c). We suggest that, due to the presence of cracks and other microscopic defects in the colloidal crystal film, the orientational correlations of mosaic blocks first increase with temperature. Then at $T > T_A$, a partial annealing process occurs and the crystal lattice becomes more relaxed. At $T > T_G$, the lattice parameter and integrated intensities of Bragg peaks sharply decrease. We attribute such behavior to the coalescence of PS particles with an increase of temperature that is revealed by the decrease of interatomic distances as discussed earlier. This is a consequence of softening of colloidal spheres at the glass transition temperature $T_G = 373$ K accompanied by interdiffusion of polymer chains.^{26,40}

5. CONCLUSIONS AND OUTLOOK

In situ X-ray diffraction studies of structural evolution of colloidal crystal films at different temperatures were performed

using the high resolution X-ray scattering setup at the P10 beamline of the PETRA III synchrotron source. The high quality colloidal crystal films formed by polystyrene spherical particles were investigated upon incremental heating in a wide temperature range from 293 to 381 K.

The structural changes in the colloidal crystal induced by incremental heating were revealed by a detailed analysis of the measured Bragg peaks. The parameters of diffraction peaks, such as the position of peak, integrated intensity, and the peak widths in radial and azimuthal directions of reciprocal space, were analyzed as a function of temperature. The Williamson–Hall method based on a mosaic block model was applied to determine the lattice distortions and the angular spread of crystalline domains in a colloidal crystal film. A significant increase of lattice distortion and domain misorientation parameters in a polystyrene colloidal crystal was revealed around the annealing temperature of 355 K. From the analysis of the form factor scattering signal and Bragg peak positions, we observed a linear behavior of the thermal expansion of PS spherical particles. The determined coefficient of thermal expansion is in good agreement with the literature data. As a result of our analysis, we have identified four stages of structural evolution of a colloidal crystal upon heating: steady state, preannealing, shape transformation, and crystal melting. We finally proposed a model of structural evolution of a colloidal crystal upon incremental heating on the nanoscopic and mesoscopic length scales.

The results of our investigation provide valuable information for fabrication process of photonic devices based on colloidal crystals and tuning their properties by changing the operating temperature. In our future work, we are aiming for the detailed study of defect behavior⁴¹ under incremental heating of colloidal crystals. Of special interest are dynamics studies of colloidal crystals in the pump–probe experiments,⁴² which could provide unique information on dynamics of the colloidal crystal film as well as on the ultrafast melting process of the polystyrene.

■ ASSOCIATED CONTENT

● Supporting Information

Details of data processing and analyses of Bragg peaks and form factor curves. This material is available free of charge via the Internet at <http://pubs.acs.org>.

■ AUTHOR INFORMATION

Corresponding Authors

*E-mail: alexey.zozulya@desy.de (A.V.Z.).

*E-mail: ivan.vartanyants@desy.de (I.A.V.).

Notes

The authors declare no competing financial interest.

ACKNOWLEDGMENTS

We acknowledge the support of the project and fruitful discussions with E. Weckert, support in the use of GNOM program provided by V. V. Volkov, and fruitful discussions with V. M. Kaganer and P. V. Konarev. We are also thankful for a careful reading of the manuscript by D. V. Novikov. This work was supported by BMBF Proposal 05K10CHG "Coherent Diffraction Imaging and Scattering of Ultrashort Coherent Pulses with Matter" in the framework of the German–Russian collaboration "Development and Use of Accelerator-Based Photon Sources" and the Virtual Institute VH-VI-403 of the Helmholtz Association. Partial funding by the Russian Foundation for Basic Research (Grant 14-22-00098) is acknowledged.

REFERENCES

- (1) Johnson, S. G.; Joannopoulos, J. D. *Photonic Crystals: The Road from Theory to Practice*; Kluwer Academic Publishers: Norwell, MA, 2002.
- (2) Denkov, N. D.; Velev, O. D.; Kralchevsky, P. A.; Ivanov, I. B.; Yoshimura, H.; Nagayama, K. Two-dimensional crystallization. *Nature* **1993**, *361*, 26.
- (3) Vlasov, Y. A.; Bo, X.-Z.; Sturm, J. C.; Norris, D. J. On-chip natural assembly of silicon photonic bandgap crystals. *Nature (London)* **2001**, *414*, 289–293.
- (4) Vlasov, Yu. A.; Astratov, V. N.; Baryshev, A. V.; Kaplyanskii, A. A.; Karimov, O. Z.; Limonov, M. F. Manifestation of intrinsic defects in optical properties of self-organized opal photonic crystals. *Phys. Rev. E* **2000**, *61*, 578.
- (5) Warren, B. E. *X-ray Diffraction*; Dover Publications: New York, 1990.
- (6) Bolhuis, P. G.; Frenkel, D.; Mau, S.-C.; Huse, D. A. Entropy difference between crystal phases. *Nature* **1997**, *388*, 235–236.
- (7) Petukhov, A. V.; Dolbnya, I. P.; Aarts, D. G. A. L.; Vroege, G. J.; Lekkerkerker, H. N. W. Bragg rods and multiple X-ray scattering in random-stacking colloidal crystals. *Phys. Rev. Lett.* **2003**, *90*, 028304.
- (8) Dolbnya, I. P.; Petukhov, A. V.; Aarts, D. G. A. L.; Vroege, G. J.; Lekkerkerker, H. N. W. Coexistence of rhcp and fcc phases in hard-sphere colloidal crystals. *Europhys. Lett.* **2005**, *72*, 962–968.
- (9) Dinsmore, A. D.; Weeks, E. R.; Prasad, V.; Levitt, A. C.; Weitz, D. A. Three-dimensional confocal microscopy of colloids. *Appl. Opt.* **2001**, *40*, 4152–4159.
- (10) Schall, P.; Cohen, I.; Weitz, D. A.; Spaepen, F. Visualization of dislocation dynamics in colloidal crystals. *Science* **2004**, *305*, 1944–1948.
- (11) Schall, P. Laser diffraction microscopy. *Rep. Prog. Phys.* **2009**, *72*, 076601.
- (12) Ye, Y.-H.; Mayer, T. S.; Khoo, I.-C.; Divliansky, I. B.; Abrams, N.; Mallouk, T. E. Self-assembly of three-dimensional photonic-crystals with air-core line defects. *J. Mater. Chem.* **2002**, *12*, 3637–3639.
- (13) Sirota, E. B.; Ou-Yang, H. D.; Sinha, S. K.; Chaikin, P. M.; Axe, J. D.; Fujii, Y. Complete phase diagram of a charged colloidal system: A synchrotron X-ray scattering study. *Phys. Rev. Lett.* **1989**, *62*, 1524.
- (14) Chen, L. B.; Chow, M. K.; Ackerson, B. J.; Zukoski, C. F. Rheological and microstructural transitions in colloidal crystals. *Langmuir* **1994**, *10*, 2817–2829.
- (15) Petukhov, A. V.; Thijssen, J. H. J.; 't Hart, D. C.; Imhof, A.; van Blaaderen, A.; Dolbnya, I. P.; Snigirev, A.; Moussaïd, A.; Snigireva, I. Microradian X-ray diffraction in colloidal photonic crystals. *J. Appl. Crystallogr.* **2006**, *39*, 137–144.
- (16) Vos, W. L.; Megens, M.; van Kats, C. M.; Bösecke, P. X-ray diffraction of photonic colloidal single crystals. *Langmuir* **1997**, *13*, 6004–6008.
- (17) Hilhorst, J.; Abramova, V. V.; Sinitskii, A.; Sapoletova, N. A.; Napolskii, K. S.; Eliseev, A. A.; Byelov, D. V.; Grigoryeva, N. A.; Vasilieva, A. V.; Bouwman, W. G.; Kvashnina, K.; Snigirev, A.; Grigoriev, S. V.; Petukhov, A. V. Double stacking faults in convectively assembled crystals of colloidal spheres. *Langmuir* **2009**, *25*, 10408–10412.
- (18) Gulden, J.; Yefanov, O. M.; Mancuso, A. P.; Abramova, V. V.; Hilhorst, J.; Byelov, D.; Snigireva, I.; Snigirev, A.; Petukhov, A. V.; Vartanyants, I. A. Coherent X-ray imaging of defects in colloidal crystals. *Phys. Rev. B* **2010**, *81*, 224105.
- (19) Gulden, J.; Yefanov, O. M.; Mancuso, A. P.; Dronyak, R.; Singer, A.; Bernátová, V.; Burkhardt, A.; Polozhentsev, O.; Soldatov, A.; Sprung, M.; Vartanyants, I. A. Three-dimensional structure of a single colloidal crystal grain studied by coherent X-ray diffraction. *Opt. Express* **2012**, *20*, 4039–4049.
- (20) Meijer, J.-M.; Shabalin, A.; Dronyak, R.; Yefanov, O. M.; Singer, A.; Kurta, R. P.; Lorenz, U.; Gorobstov, O.; Dzhigaev, D.; Gulden, J.; Byelov, D. V.; Zozulya, A. V.; Sprung, M.; Vartanyants, I. A.; Petukhov, A. V. Double hexagonal close-packed structure revealed in a single colloidal crystal grain by Bragg rod analysis. *J. Appl. Crystallogr.* **2014**, *47*, 1199–1204.
- (21) Miguez, H.; Meseguer, F.; López, C.; Blanco, A.; Moya, J. S.; Requena, J.; Miñsud, A.; Fornés, V. Control of the photonic crystal properties of fcc packed submicrometric SiO₂ spheres by sintering. *Adv. Mater.* **1998**, *10*, 480–483.
- (22) Gates, B.; Park, S. H.; Younan, X. Tuning the photonic bandgap properties of crystalline arrays of polystyrene beads by annealing at elevated temperatures. *Adv. Mater.* **2000**, *12*, 653–656.
- (23) Kosiorsek, A.; Kandulski, W.; Glaczynska, H.; Giersig, M. Fabrication of nanoscale rings, dots, and rods by combining shadow nanosphere lithography and annealed polystyrene nanosphere masks. *Small* **2005**, *1*, 439–444.
- (24) Hu, S.; Rieger, J.; Roth, S. V.; Gehrke, R.; Leyrer, R. J.; Men, Y. GIUSAXS and AFM studies on surface reconstruction of latex thin films during thermal treatment. *Langmuir* **2009**, *25*, 4230–4234.
- (25) Hu, S.; Rieger, J.; Yi, Z.; Zhang, J.; Chen, X.; Roth, S. V.; Gehrke, R.; Men, Y. Structural evolution of a colloidal crystal fiber during heating and annealing studied by in situ synchrotron small angle X-ray scattering. *Langmuir* **2010**, *26*, 13216–13220.
- (26) Chen, X.; Fischer, S.; Yi, Z.; Boyko, V.; Terrenoire, A.; Reinhold, F.; Rieger, J.; Li, X.; Men, Y. Structural reorganization of a polymeric latex film during dry sintering at elevated temperatures. *Langmuir* **2011**, *27*, 8458–8463.
- (27) Herzog, G.; Abul Kashem, M. M.; Benecke, G.; Buffet, A.; Gehrke, R.; Perlich, J.; Schwartzkopf, M.; Körtgens, V.; Meier, R.; Niedermeier, M. A.; Rawolle, M.; Ruderer, M. A.; Müller-Buschbaum, P.; Wurth, W.; Roth, S. V. Influence of nanoparticle surface functionalization on the thermal stability of colloidal polystyrene films. *Langmuir* **2012**, *28*, 8230–8237.
- (28) Geng, C.; Zheng, L.; Yu, J.; Yan, Q.; Wei, T.; Wang, X.; Shen, D. Thermal annealing of colloidal monolayer at the air/water interface: A facile approach to transferrable colloidal masks with tunable interstice size for nanosphere lithography. *J. Mater. Chem.* **2012**, *22*, 22678–22685.
- (29) Zozulya, A. V.; Meijer, J.-M.; Shabalin, A.; Ricci, A.; Westermeier, F.; Kurta, R. P.; Lorenz, U.; Singer, A.; Yefanov, O.; Petukhov, A. V.; Sprung, M.; Vartanyants, I. A. In situ X-ray crystallographic study of the structural evolution of colloidal crystals upon heating. *J. Appl. Crystallogr.* **2013**, *46*, 903–907.
- (30) Jiang, P.; Bertone, J. F.; Hwang, K. S.; Colvin, V. L. Single-crystal colloidal multilayers of controlled thickness. *Chem. Mater.* **1999**, *11*, 2132–2140.
- (31) *Polymer Data Handbook*, 2nd ed.; Mark, J. E., Ed.; Oxford University Press: New York, 2009.
- (32) Zozulya, A. V.; Bondarenko, S.; Schavkan, A.; Westermeier, F.; Grübel, G.; Sprung, M. Microfocusing transfocator for 1D and 2D compound refractive lenses. *Opt. Express* **2012**, *20*, 18967–18976.

- (33) Rodenburg, J. M.; Hurst, A. C.; Cullis, A. G.; Dobson, B. R.; Pfeiffer, F.; Bunk, O.; David, C.; Jefimovs, K.; Johnson, I. Hard-X-ray lensless imaging of extended objects. *Phys. Rev. Lett.* **2007**, *98*, 034801.
- (34) Thibault, P.; Dierolf, M.; Menzel, A.; Bunk, O.; David, C.; Pfeiffer, F. High-resolution scanning X-ray diffraction microscopy. *Science* **2008**, *321*, 379.
- (35) Sutton, M.; Mochrie, S. G. J.; Greytak, T.; Nagler, S. E.; Berman, L. E.; Held, G. A.; Stephenson, G. B. Observation of speckle by diffraction with coherent X-rays. *Nature* **1991**, *352*, 608–610.
- (36) Alsayed, A. M.; Islam, M. F.; Zhang, J.; Collings, P. J.; Yodh, A. G. Premelting at defects within bulk colloidal crystals. *Science* **2005**, *309*, 1207.
- (37) Williamson, G.K.; Hall, W.H. X-ray line broadening from filed aluminium and wolfram. *Acta Metall.* **1953**, *1*, 23–31.
- (38) Moram, M. A.; Vickers, M. E. X-ray diffraction of III-nitrides. *Rep. Prog. Phys.* **2009**, *72*, 036502.
- (39) Turner, P.S. Thermal-expansion stresses in reinforced plastics. *J. Res. Natl. Bur. Stand.* **1946**, *37*, 239–250.
- (40) Boczar, E. M.; Dionne, B. C.; Fu, Z.; Kirk, A. B.; Lesko, P. M.; Koller, A. D. Spectroscopic studies of polymer interdiffusion during film formation. *Macromolecules* **1993**, *26*, 5772–5781.
- (41) Krivoglaz, M. A. *Diffuse Scattering of X-Rays and Neutrons by Fluctuations*; Springer: Berlin, 1996.
- (42) Dronyak, R.; AAGulden, J.; Yefanov, O. M.; Singer, A.; Gorniak, T.; Senkbeil, T.; Meijer, J.-M.; Al-Shemmary, A.; Hallmann, J.; Mai, D. D.; Reusch, T.; Dzhigaev, D.; Kurta, R. P.; Lorenz, U.; Petukhov, A. V.; Düsterer, S.; Treusch, R.; Strikhanov, M. N.; Weckert, E.; Mancuso, A. P.; Salditt, T.; Rosenhahn, A.; Vartanyants, I. A. Dynamics of colloidal crystals studied by pump-probe experiments at FLASH. *Phys. Rev. B* **2012**, *86*, 064303.